Journal of
Marine Science and Engineering

MDPI

Article

Effect of Square Cap on Pile-Group Wave Force: Parametric Analysis and Case Study

Rujin Ma, Yi Liu, Haocheng Chang * and Zhenkun Hong

College of Civil Engineering, Tongji University, Shanghai 200092, China
* Correspondence: changhc16@tongji.edu.cn

Abstract: The square cap is a typical semi-submersible component of sea-crossing bridges, which connects piers and pile-group foundations. As the cap size is large, it usually has a non-negligible influence on the wave motion around the pile-group foundation, so it is not considered in the relevant specification. However, neglecting this influence may have adverse effects on the structure. In this paper, the wave forces on capped pile groups are simulated by a numerical wave flume. Firstly, the numerical flume used in this paper is validated by an experiment in the previous literature. Then, capped pile groups with different arrangements and different water levels are modeled to study the interference effect of the square cap on the wave force, and the variation law of the interference effect coefficient K_{cp} of the cap is given. Next, we introduce K_{cp} into the theoretical formula of wave forces on pile groups and obtain a modified formula that considers the cap effect. To verify the feasibility of the modified formula in practical engineering, we use the formula to calculate the wave forces acting on capped pile groups of a sea-crossing bridge. The results of the modified theoretical formula are compared with that of the numerical water flume and recommended values in the specification. It is found that the theoretical values are relatively close to the numerical results, while the specification values tend to be conservative. The modified theoretical formula proposed in this paper and the obtained parameter distribution law can provide a reference for engineering design.

Keywords: wave force; cap effect; sea-crossing bridge; pile-group foundation; cap-interference coefficient

Citation: Ma, R.; Liu, Y.; Chang, H.; Hong, Z. Effect of Square Cap on Pile-Group Wave Force: Parametric Analysis and Case Study. *J. Mar. Sci. Eng.* **2023**, *11*, 1677. https://doi.org/10.3390/jmse11091677

Academic Editors: Barbara Zanuttigh and José António Correia

Received: 13 July 2023
Revised: 7 August 2023
Accepted: 23 August 2023
Published: 25 August 2023

1. Introduction

In recent years, numerous sea-crossing bridges have been constructed worldwide. However, during the life cycle of these bridges, the harsh marine environment [1], including hurricanes and ocean currents, can severely impact their service life and even cause instability or structural damage [2], leading to potentially disastrous safety incidents. Most highway bridge destruction can be attributed to bridge collapse due to wave load impacts [3]. Consequently, the design of wave load on the foundation structure of a sea-crossing bridge has emerged as a key component of the entire bridge design. Wave force is influenced by environmental factors such as water level and flow velocity as well as factors such as pile group arrangement, pile diameter, and cap size [4].

In the last century, scholars began conducting extensive research on calculating wave force on the pile-group foundations of sea-crossing bridges [5,6]. The Morison formula [7], derived from potential flow theory, is one of the most famous semi-theoretical formulas for calculating horizontal wave force on a small-scale vertical cylinder. However, the hydrodynamic coefficients for the inertial force and drag force in the formula are affected by various factors such as the Reynolds number and KC number, and their values must be determined precisely through experiments [8], which has paved the way for the development of related experimental research. Thereafter, Sarpkaya and Justesen [9,10] obtained the force coefficient through numerous wave flume experiments. Based on their work, Boccotti [11] conducted further experiments to study how the coefficients vary with the KC

number and Re number. It is worth noting that the Morison formula is no longer applicable to large-scale structures such as pile groups and foundations, as waves reflect and diffract between such structures. MacCamy [12] first proposed a diffraction theory based on the assumption of small-amplitude linear waves. Neelamani [13] further verified the accuracy of the diffraction theory by carrying out a water flume test. Garrison [14] has also regulated the Morison equation and diffraction theory's applicable range. Terro [15] modified the linear form of the Morison equation based on the numerical water flume, making it more accurate for nonlinear wave force estimation.

Although significant improvements have been made to theoretical methods, their application is still limited. For such cases, the physical water flume experiment is an appealing solution. Liu [16] used a three-dimensional flume to determine the reduction coefficient of the wave force on a pile group by analyzing the force of four different types of inclined piles on the East Sea Bridge. Qu [17] proposed a method to assess the total wave force using the effective diameter, which was determined through wave flume experiments. Based on this, an empirical formula was developed to calculate the wave force of various pile-supported structures in regular and irregular waves. Zhang [18,19] conducted wave flume experiments to study the wave force on pile groups with different arrangements under varying wave conditions. Moreover, Bonakdar [20] used an artificial intelligence data analysis method to derive a new calculation formula for pile-group wave force based on wave flume experiments. However, the physical experiment is costly and has low universality, which brings many inconveniences to researchers when a large number of experiments are needed.

With the progress of computer technology, numerical flumes have developed rapidly, greatly reducing the time, economic costs, and labor costs required for experiments. Many scholars have also verified the accuracy of the numerical flume through comparisons with physical experiments [21]. Dong [22] studied the generation and propagation of the wave in a numerical viscous wave flume and accurately generated several incident waves. Huang [23] created a two-dimensional wave–current interaction model and then proposed an empirical equation for the wave–current force acting on a box girder bridge. Deng [24] investigated the influences of wave height, wave length, cap dimension, and submerged depth on the cap effects through a numerical water flume. All these lay the foundation for solving the wave force of the pile group by numerical flume. However, research on the interaction between the cap and the pile group is limited, and the influence of pile arrangements and water levels on wave forces is rarely considered.

This paper aims to reveal the influence of the cap on wave forces acting on pile groups through a three-dimensional numerical water flume. The remainder of this paper is organized as follows. Section 2 briefly introduces the numerical methods used and the validation of the numerical flume, including wave generation and elimination, the grid size, and the boundary conditions. The numerical flume has been validated with the test results of the physical flume in the relevant literature. In Section 3, the influence of the cap on the wave forces acting on the pile group with different arrangements and water levels is studied. In Section 4, we establish a modified theoretical formula for calculating wave forces considering the cap effect. In Section 5, an engineering project is simulated to verify the feasibility of the modified theoretical formula proposed in this paper. Conclusions are drawn in Section 6.

2. Numerical Methods and Validation

2.1. Numerical Methods

2.1.1. Governing Equations

The governing equations for our fluid simulation include the continuity equation and momentum equation [25]:

$$\frac{\partial \rho}{\partial t} + \nabla \cdot (\rho \boldsymbol{u}) = 0 \tag{1}$$

$$\frac{\partial(\rho u_i)}{\partial t} + \nabla(\rho u_i \boldsymbol{u}) = \nabla(\mu \mathrm{grad} u_i) - \frac{\partial p}{\partial x_i} + S_{u_i} \tag{2}$$

in which ρ is the density of fluid; $\boldsymbol{u}$ is the velocity vector and u_i are fluctuating velocity components; and p is pressure. μ is viscosity coefficient; grad = $\frac{\partial}{\partial x} + \frac{\partial}{\partial y} + \frac{\partial}{\partial z}$ is the gradient; and S_{u_i} is the generalized source term of the momentum conservation equation.

The Reynolds-averaged Navier–Stokes (RANS) equations are the most widely used method for turbulence. This model establishes assumptions about the Reynolds stress through turbulence theory and observations, generating a series of empirical or semi-empirical constitutive relations that enable the closure of the motion equation of turbulence. Temperature changes are ignored in this analysis, conducted at room temperature. The conservations of the mass and momentum in the RANS equations are as follows:

$$\frac{\partial \rho}{\partial t} + \frac{\partial}{\partial x_i}(\rho u_i) = 0 \tag{3}$$

$$\frac{\partial(\rho u_i)}{\partial t} + \frac{\partial}{\partial x_j}(\rho u_i u_j) = -\frac{\partial p}{\partial x_i} + \rho g_i + \frac{\partial}{\partial x_j}[\mu\left(\frac{\partial u_i}{\partial x_j} + \frac{\partial u_j}{\partial x_i}\right) - \rho\overline{u_i' u_j'}] \tag{4}$$

in which i and j represent the directions of the coordinates $(x; y; z)$; g_i is the acceleration; $\rho\overline{u_i' u_j'}$ is the Reynolds stress which represents the effects of the turbulent flow on the mean flow field. Recently, the RANS method has been applied to wave simulation and has achieved good results [26]. Finnegan [27] compared turbulence flow models and found that there was no difference in the height of waves generated between the models, so the turbulence model is not a factor in the generation of waves using a wave-maker. In addition, in this article, we chose the k-ω model [28,29].

2.1.2. Volume-of-Fluid Method

Establishing a numerical flume also requires an accurate description of the free surface, that is, the interface between the air and water phases [30]. This paper uses the volume-of-fluid (VOF) method. The VOF method introduces a fluid volume fraction, α_n, defined as the ratio of the volume of the n-th phase fluid to the total volume of the grid in a certain grid. The numerical wave flume established in this paper only involves two phases, air and water, as schematically shown in Figure 1. The free surface can be described as follows:

$$\alpha_2 = \begin{cases} 0, \text{ air} \\ 0 < \alpha_2 < 1, \text{ free surface} \\ 1, \text{ water} \end{cases} \tag{5}$$

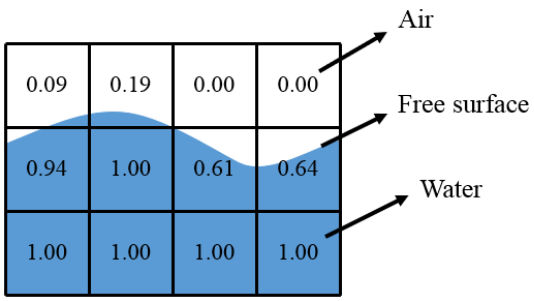

Figure 1. Diagram of the VOF method.

Free surfaces are extracted from $\alpha_2 = 0.5$. The following equations must be satisfied by the volume fraction α_n:

$$\begin{cases} \frac{\partial \alpha_n}{\partial t} + \frac{\partial (u\alpha_n)}{\partial x} + \frac{\partial (v\alpha_n)}{\partial y} = 0 \\ \sum_{n=1}^{2} \alpha_n = 1 \end{cases} \quad n = 1, 2 \tag{6}$$

2.2. Validation of the Numerical Wave Flume

The thickness of the boundary layer grid on the surface of the structure will have an impact on the results. In this section, we first verify the sensitivity of the numerical grid. This section selects a two-dimensional cylindrical flow for research, and liquid water is used as the fluid. The boundary layer grid thickness and the overall grid are simulated and analyzed for size impact, in which $D/200$, $D/125$, $D/100$, $D/80$, $D/50$, $D/25$, and $D/20$ are selected for the boundary layer grid, and $D/10$ is selected for the overall grid, in which D is the diameter of the cylinder. The grid of the $D/100$ boundary layer is shown in Figure 2.

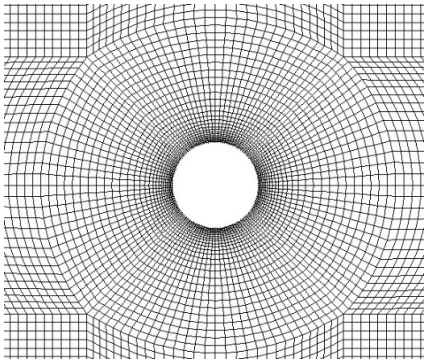

Figure 2. The grid of the $D/100$ boundary layer.

Calculate the drag coefficient of different simulation results according to the following formula:

$$F_D = \frac{1}{2} C_D \rho U^2 D \tag{7}$$

in which F_D is the cylinder resistance. The C_D results of different cases of boundary layer grid thickness are shown in Figure 3. It can be seen from the results that when the boundary layer grid thickness is less than or equal to $D/100$, the error between the simulated value and the value in reference [31] is already small, so the boundary layer thickness of about $D/100$ can be used in the simulation to obtain more accurate results.

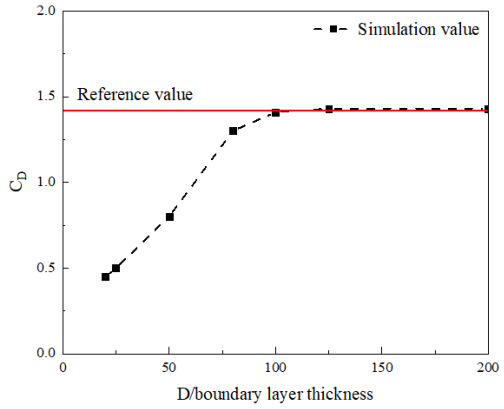

Figure 3. Simulation results of different boundary layer thicknesses.

A comparison between the numerical wave flume and the corresponding physical experiment [32] is made here to validate the numerical wave flume. The experimental setup involves a wave flume with a depth of 7 m, a width of 5 m, and an effective length of 309 m. For the experiment, a cylinder with a diameter of 0.7 m is positioned 110 m away from the wave-generating plate, with wave gauges, strain gauges, current meters, and pressure cells arranged on the cylinder. The wave parameters are presented in Table 1. The test device is shown in Figure 4. We used ANSYS Fluent 19.0 to establish the numerical water flume.

Table 1. Wave parameters for validation.

Wave Type	Depth *d*/m	Period *T*/s	Wave Height *H*/m	Wave Number*k*/m^{-1}
Regular wave	4.76	4	1.2	0.2735

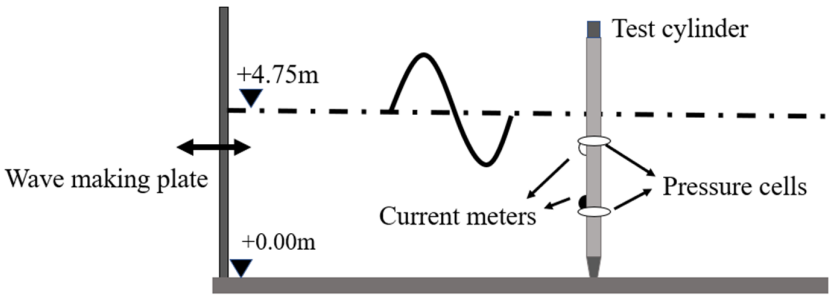

Figure 4. Wave flume test device [32].

As depicted in Figure 5, the numerical wave flume utilized in this study possesses a length of 160 m, a width of 5 m, and a height of 8 m. The distance between the structure and the inlet is 40 m. The inlet is designated as the velocity inlet, while the outlet and top are the pressure outlets. Symmetrical boundaries are assigned to the flume's two sides, while non-slip boundaries are used for the column and the bottom. The overall grid size is set as $D/10$, whereas the grid size of the cylinder and the bottom boundary layer is set as $D/100$, as illustrated in Figure 6 [33]. Three pressure measuring points are arranged in the same positions as those of the experiment, pressure$_{0^\circ}$, pressure$_{90^\circ}$, and pressure$_{180^\circ}$. In addition, the time interval is 0.01 s.

Furthermore, the paper utilizes an absorption zone to eliminate the wave reflection on the outlet boundary [34]. Specifically, an artificial damping term is added to the momentum equation [35]. A schematic diagram of the numerical water flume is shown in Figure 7.

For wave generation, the velocity distribution of the water points and wave surface at the entrance are set according to the Fenton formula [36] to generate regular waves. A comparison between the experiment results and the numerical results of the three pressure measuring points, $pressure_{0^\circ}$, $pressure_{90^\circ}$, and $pressure_{180^\circ}$, is presented in Figure 8a–c. Dynamic pressure refers to the total pressure minus the static pressure. A comparison of the total wave force on the single pile is also displayed in Figure 8d.

It can be seen that the results obtained by the numerical water flume are uniform sine waves in the stable stage, while the actual test is influenced by the equipment and instruments, and the results are not completely consistent within each cycle. However, as depicted in these graphs, the error between the numerical and experimental results is negligible. The results of the threedimensional numerical wave flume established in this paper are consistent with the corresponding experiment results. Hence, utilizing the numerical wave flume to investigate structures' wave forces is reliable.

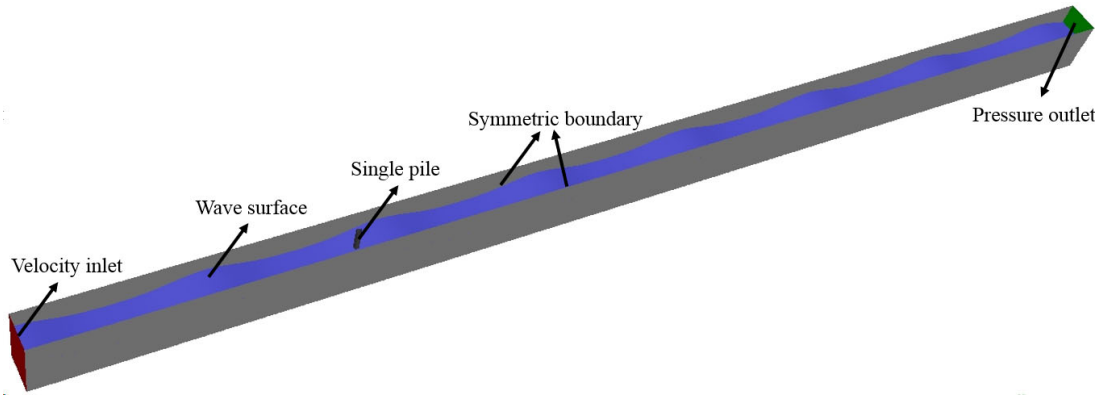

Figure 5. Three-dimensional numerical flume of verification test.

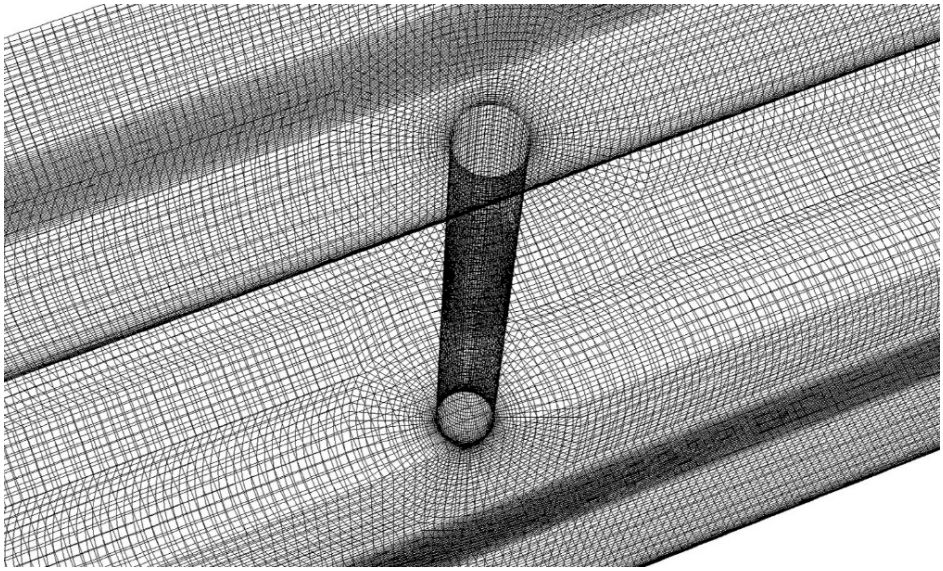

Figure 6. Local diagram of mesh.

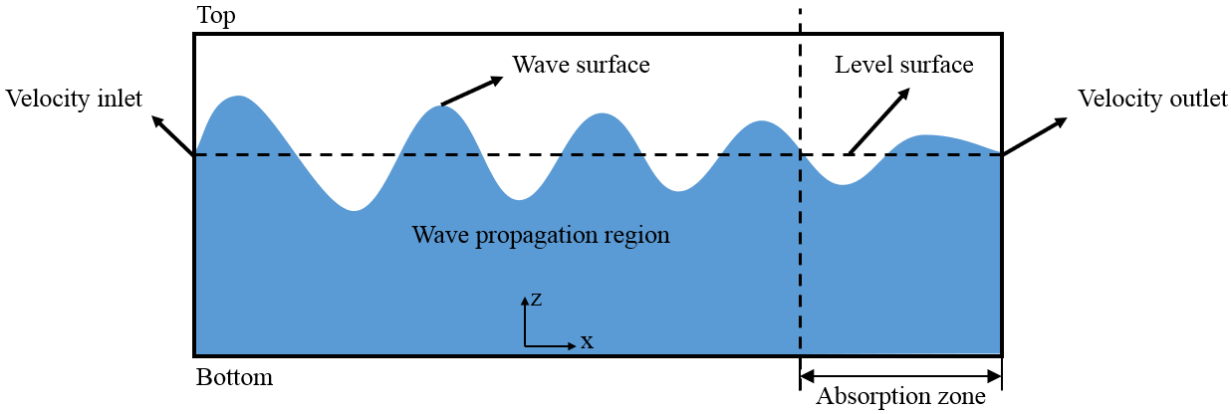

Figure 7. Schematic diagram of the numerical water flume.

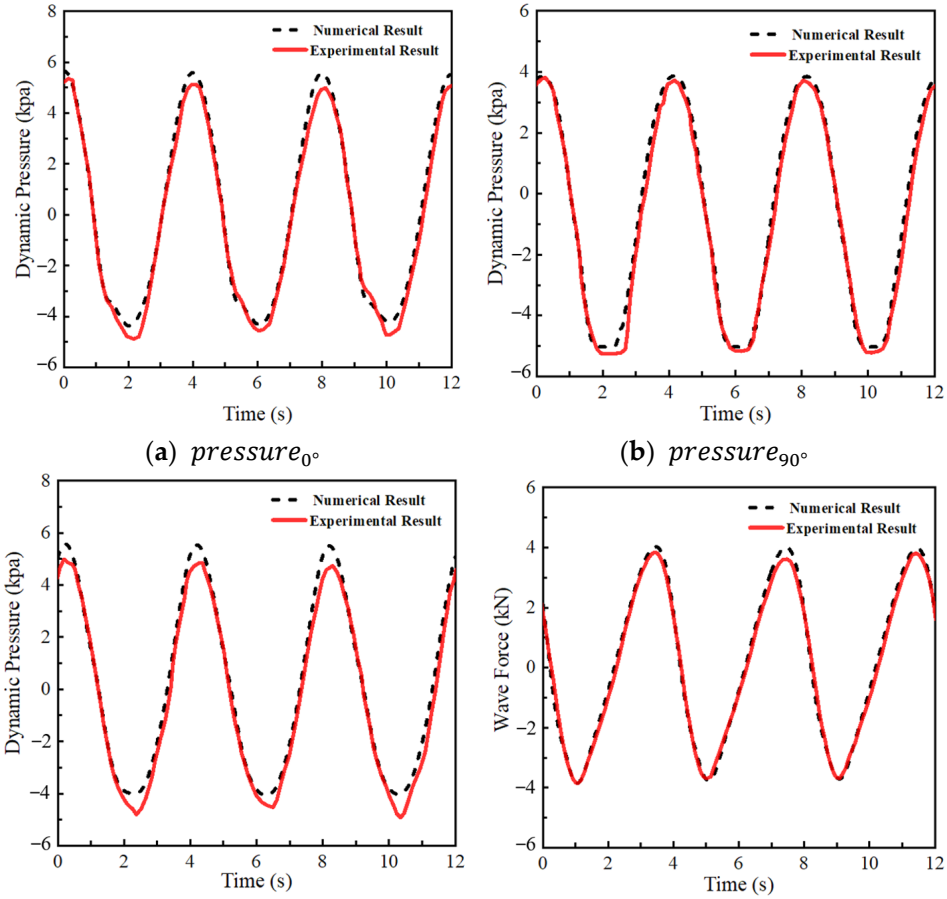

Figure 8. Comparison of pressure and wave force time history in test and numerical simulation.

3. The Influence of Different Pile Arrangements and Water Levels

A bridge's pile-group foundation structure typically comprises two components: the cap and the pile group. A large cap can cause significant disruption to the surrounding wave field, thereby affecting the wave force on the pile group. In this section, the numerical wave flume is applied to study the effect of caps on pile-group wave forces across various pile arrangements and water levels.

3.1. Different Arrangements

Three different capped pile groups are simulated: two piles arranged in the vertical wave direction, two piles parallel to the wave direction, and four piles arranged in two rows and two columns. The parameters of the three cases are shown in Table 2. Three different distances between the pile centers are investigated. Fifth-order Stokes waves with a wave height of 0.73 m and a wavelength of 15 m are utilized. The water level is set at the midpoint of the cap height, and the water-level coefficient C_w is 0.5. The length of the numerical wave flume is 60 m, and the water depth is 7 m. The pile-group foundation structure is set at a distance of 20 m from the wave-making inlet. Only the meshing of case 6 is shown in Figure 9a. The wave surface velocity contour of the numerical flume at a certain time under three arrangement cases are shown in Figure 9b–d (cases 1, 3, and 6), respectively.

Table 2. Simulation cases of capped pile group.

Case	Arrangement	Pile Diameter /m	Center Distance of Pile *l*/m	Height of Cap *h*/m	Width of Cap *b*/m	Length of Cap *L*/m
1	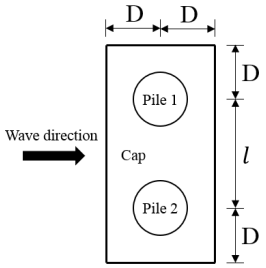	1	2	1	4	2
2		1	3	1	5	2
3	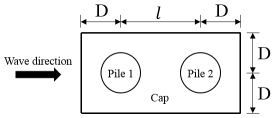	1	2	1	2	4
4		1	3	1	2	5
5		1	4	1	2	6
6	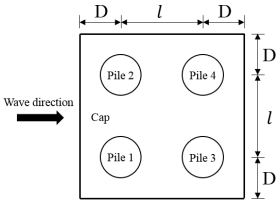	1	2	1	4	4
7		1	3	1	5	5

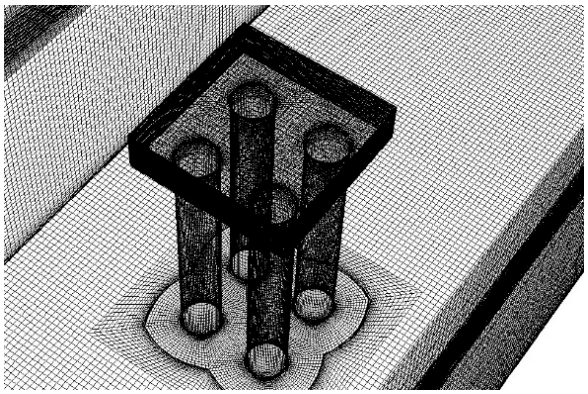

(**a**) Meshing

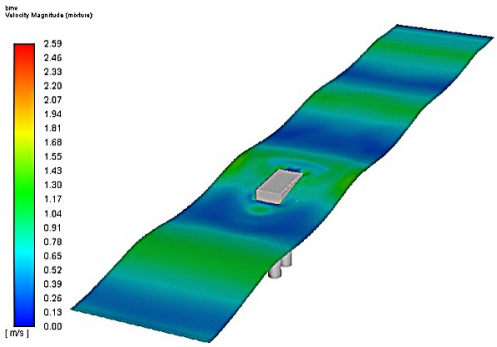

(**b**) Case 1

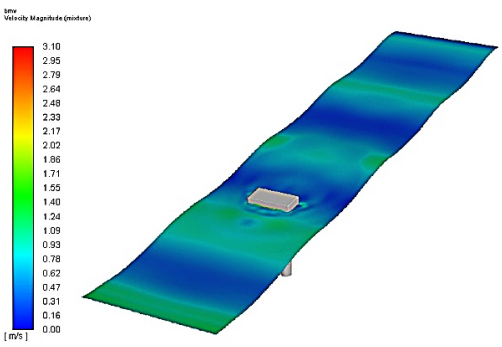

(**c**) Case 3

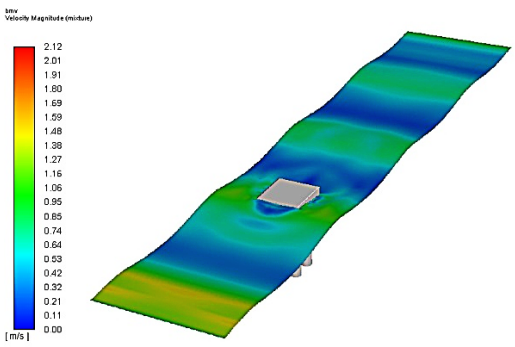

(**d**) Case 6

Figure 9. Meshing diagram and numerical flume diagram of capped pile group.

3.1.1. Two Piles Arranged in Vertical Wave Direction

The initial two simulation cases feature two piles arranged in the vertical wave direction, albeit with different distances between their centers. We can obtain the wave-force time histories for each pile, which we can then compare to those obtained without a cap for the same cases. The comparisons are displayed in Figure 10. As shown in Figure 8, each capped pile experiences a decreased wave force compared to the uncapped scenario. Moreover, the cap structure has a more pronounced reduction effect on the peak value of the wave force than the valley value.

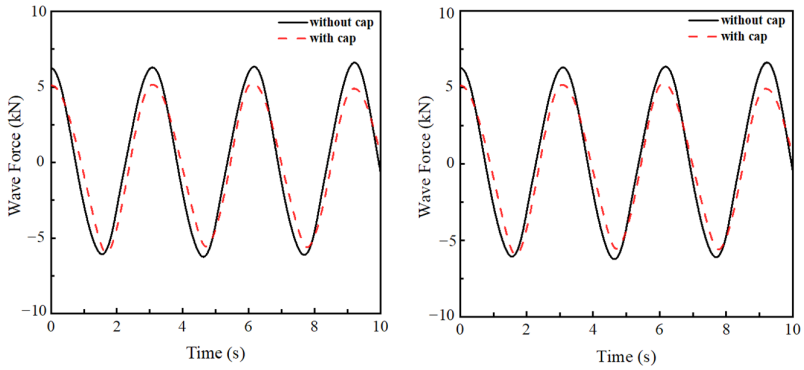

(**a**) Pile 1 of case 1 (**b**) Pile 2 of case 2

Figure 10. Comparison of wave-force time history of two piles arranged in the vertical wave direction with or without pile cap.

The interference coefficient K_{cp} of the cap on the pile can be defined as follows:

$$K_{cp} = \frac{F_{with\ cap}}{F_{without\ cap}} \tag{8}$$

where $F_{with\ cap}$ is the extreme value of wave force on capped piles, and $F_{without\ cap}$ is that on piles without a cap. The average values of the peak and valley values of the wave forces of the two piles in the above cases are obtained as shown in Table 3, as well as K_{cp}.

Table 3. Cap-interference coefficient of multiple capped piles arranged in vertical wave direction.

Pile Number	Center Distance of Pile	Wave Force without Cap/kN		Wave Force with Cap/kN		Cap-Interference Coefficient K_{cp}	
		Peak Value	Valley Value	Peak Value	Valley Value	Peak Value	Valley Value
1	2*D*	6.42	6.32	5.22	5.65	0.81	0.89
	3*D*	6.12	6.05	4.95	5.62	0.81	0.93
2	2*D*	6.42	6.32	5.23	5.65	0.81	0.90
	3*D*	6.12	6.05	4.96	5.62	0.81	0.93

We can infer from Table 3 that the position of the pile, the distance between pile centers, and the width of the pile have little effect on the cap-interference coefficient of the peak wave force when arranged in the vertical wave direction. It is worth noting that the interference coefficient of the peak value is lower than that of the valley value as the cap has more noticeable interference effects on the peak wave force.

3.1.2. Two Piles Arranged in Parallel Wave Direction

Cases 3 to 5 are two piles arranged in parallel wave directions with different pile-center distances. Compared with the corresponding non-cap case results, the cap-interference coefficient is calculated as shown in Table 4.

Table 4. Cap-interference coefficient of multiple capped piles arranged in parallel wave direction.

Pile Number	Center Distance of Pile	Wave Force without Cap/kN		Wave Force with Cap/kN		Cap-Interference Coefficient K_{cp}	
		Peak Value	Valley Value	Peak Value	Valley Value	Peak Value	Valley Value
1	2*D*	4.98	5.33	3.80	4.27	0.76	0.80
	3*D*	5.25	5.44	3.82	4.17	0.73	0.77
	4*D*	5.83	6.01	4.04	4.43	0.69	0.74
2	2*D*	5.23	5.32	4.13	4.31	0.79	0.81
	3*D*	5.40	5.49	4.17	4.39	0.77	0.80
	4*D*	5.78	5.95	4.39	4.61	0.76	0.78

As shown in Table 4, the interference coefficient of the cap for front pile 1 decreases as the distance between pile centers increases. Similarly, there is a modest decrease in the interference coefficient of the cap for rear pile 2 as the distance between pile centers expands.

It can be observed that different pile-center distances have distinct impacts in the case of two piles arranged in the parallel wave direction. For pile 1, the center distance will change the length of its rear cap, without affecting the length of its front cap; for pile 2, the center distance will change the length of its front cap without affecting the length of its rear cap. For convenience, we define the cap length on the front side of the pile, denoted by d_f, as the distance from the pile center to the front side of the cap and, similarly, the cap length on the backside of the pile, denoted by d_b, as the distance from the pile center to the backside of the cap.

(1) The influence of d_b on the cap-interference coefficient.

Based on our analysis of the cap-interference coefficient of two piles arranged in the vertical wave direction in the previous section, we observed that the lateral position and width of the cap have minimal effects on the cap-interference coefficient of the two piles. Rather, the length of the cap on either side of the pile significantly affects the cap-interference coefficient. By combining the results in this section, we can depict the changes in the cap-interference coefficient of pile 1 as a function of the length of the cap at the back of the pile, as illustrated in Figure 11.

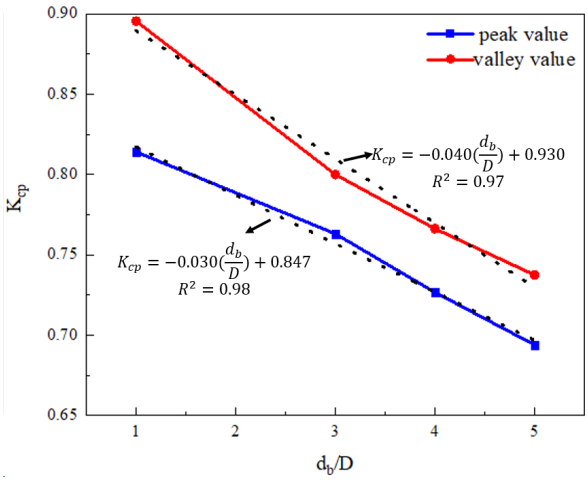

Figure 11. The variation of the interference coefficient of the cap with the length of the cap at the back of the pile.

As shown in the figure, when the length of the cap on the front side of the pile remains constant, the interference coefficient decreases as the length of the cap on the backside of the pile increases. In other words, the greater the length of the cap on the backside, the stronger the interference effect. Moreover, we observe that the interference coefficient of the wave-force valley value is slightly larger than that of the peak value.

(2) The influence of d_f on the cap-interference coefficient.

Likewise, we present the changes in the cap-interference coefficient of pile 2 in Figure 12. It is apparent that when the length of the cap behind the pile remains constant, the cap-interference coefficient increases as the length of the cap in front of the pile extends. Moreover, we notice that the interference coefficient of the wave-force valley value is slightly greater than that of the peak value.

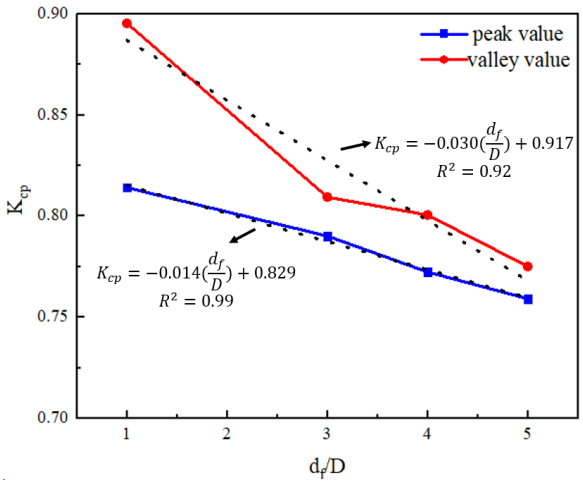

Figure 12. The variation of the interference coefficient of the cap with the length of the cap in the front of the pile.

3.1.3. Four Piles Arranged in Two Rows and Two Columns

Cases 6 and 7 are four piles arranged in two rows and two columns with different pile-center distances. Compared with the corresponding non-cap case results, the cap-interference coefficient is calculated as shown in Table 5.

Table 5. Cap-interference coefficient of multiple capped piles arranged in two rows and two columns.

Pile Number	Center Distance of Pile	Wave Force without Cap/kN		Wave Force with Cap/kN		Cap-Interference Coefficient K_{cp}	
		Peak Value	Valley Value	Peak Value	Valley Value	Peak Value	Valley Value
1	2*D*	5.29	5.53	3.96	4.44	0.75	0.80
	3*D*	5.53	5.51	4.04	4.22	0.73	0.77
2	2*D*	5.25	5.52	3.93	4.44	0.75	0.80
	3*D*	5.51	5.45	4.04	4.22	0.73	0.77
3	2*D*	5.67	5.71	4.40	4.52	0.78	0.79
	3*D*	5.66	5.64	4.27	4.42	0.75	0.78
4	2*D*	5.75	5.64	4.47	4.48	0.78	0.79
	3*D*	5.66	5.64	4.27	4.42	0.75	0.78

It is apparent from Table 5 that the interference coefficients of the adjacent piles (pile 1 and pile 2, as well as pile 3 and pile 4) in the vertical wave direction are equal, implying that the location of different vertical wave directions does not affect the cap-interference coefficient. On the other hand, the arrangement positions of the piles in the parallel wave direction and the pile-center distances influence the cap-interference coefficient. As presented in Table 6, we compare the cap-interference coefficients of pile 1 and pile 3 arranged in the parallel wave direction of this section with those of the two piles in cases 4 and 5. Table 6 indicates that the two arrangements' interference effect coefficients of the corresponding pile positions are the same. Thus, for multi-row capped pile groups, we can calculate the cap-interference coefficient of each row of piles in the parallel wave direction based on the corresponding single row of piles.

Table 6. Comparison of interference coefficients between two piles arranged in parallel wave direction and four piles arranged in two rows and two columns.

Pile Position	Center Distance of Pile	Peak Value			Valley Value		
		Two Piles	Four Piles	Error	Two Piles	Four Piles	Error
Front	2D	0.76	0.75	−1.32%	0.80	0.80	−0.35%
	3D	0.73	0.73	−0.45%	0.77	0.77	−0.04%
Rear	2D	0.79	0.78	−1.27%	0.81	0.79	−2.47%
	3D	0.77	0.76	−1.30%	0.80	0.78	−2.50%

3.2. Different Water Levels

When the cap's submerged depth varies, so does the interference with the pile group. In this section, the two capped piles arranged in the vertical wave direction with three different water-level coefficients are simulated. The simulation cases are shown in Table 7. The wave distribution contour along the wave-direction section of pile 1 in the simulation is shown in Figure 13.

Table 7. Simulation cases of different water levels.

Case	Water-Level Coefficient C_W	Pile Diameter D/m	Center Distance of Pile l	Height of Cap h/m	Width of Cap b/m	Length of Cap b/m
1	0	1	$2D$	1	4	2
2	0.5	1	$2D$	1	4	2
3	1.0	1	$2D$	1	4	2

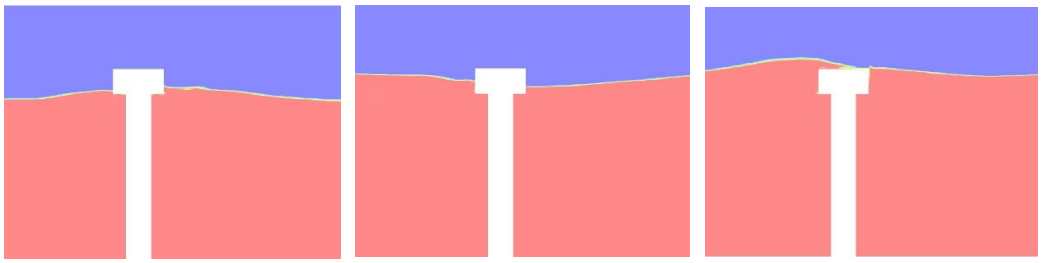

(**a**) $C_W = 0$ (**b**) $C_W = 0.5$ (**c**) $C_W = 1$

Figure 13. The wave distribution contour along the wave-direction section of pile 1 in the simulation.

We obtain the wave-force time history of the two piles in three cases, which is then compared with the results of the corresponding non-cap situation, as illustrated in Figure 14. It is observable from the figure that when the cap is not submerged, the extreme value of the wave force on the pile is similar to the corresponding result of the non-cap case. As the cap's submerged depth increases, the cap's interference on the pile's wave force also elevates.

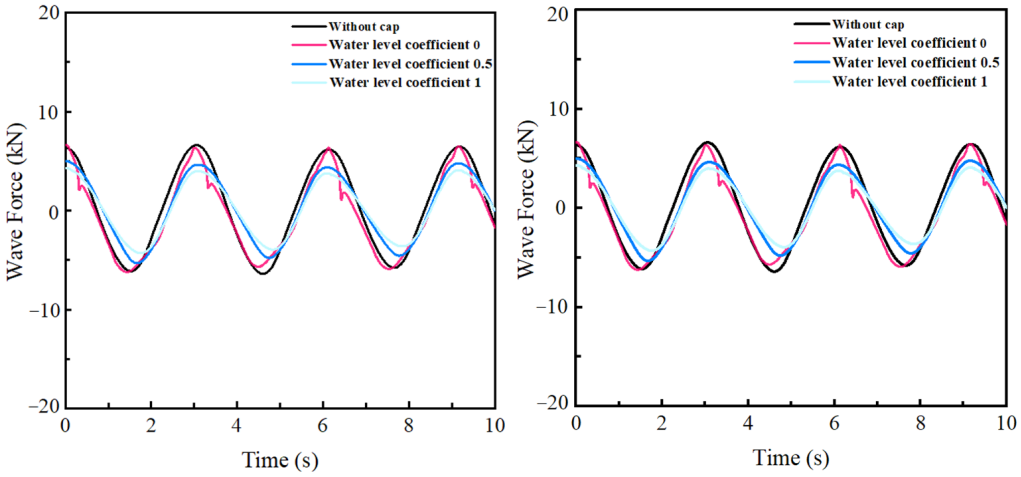

(**a**) Pile 1 (**b**) Pile 2

Figure 14. Comparison of wave-force time history of two piles arranged in vertical wave direction at different water levels.

Table 8 displays the result of the cap-interference coefficient of the two piles in various water-level scenarios. It can be observed that the cap-interference coefficients of pile 1 and pile 2 are identical. Moreover, the interference effect of the cap strengthens with an increase in the water-level coefficient, leading to a decrease in the cap-interference coefficient.

Table 8. The cap-interference coefficient K_{cp} of different water levels.

Water-Level Coefficient C_W	Pile 1		Pile 2	
	Peak Value	Valley Value	Peak Value	Valley Value
0	1.00	0.96	1.00	0.96
0.5	0.81	0.89	0.81	0.89
1.0	0.63	0.63	0.63	0.63

4. Modified Theoretical Formula for Calculating Wave Forces Considering Cap Effect

We introduce K_{cp} into the theoretical formula of wave forces on pile groups [37], which can be expressed as follows:

$$F_p(t) = \sum K_{cp} K_S K_I \cdot F_i(t) \tag{9}$$

where $F_p(t)$ is the wave-force time history of the whole pile group, and $F_i(t)$ is the wave-force time history of every single pile calculated by the Morison formula. K_{cp} is the cap-interference coefficient. K_S is the shelter effect coefficient. K_I is the interference effect coefficient.

The shelter effect coefficient K_S can be calculated as follows:

$$K_S = \frac{F_{c1}}{F_s} \tag{10}$$

where F_{c1} is the wave force of a single pile in the pile group arranged in the parallel wave direction, and F_s is the wave force on a single pile.

Similarly, the interference effect coefficient K_I can be calculated as follows:

$$K_I = \frac{F_{c2}}{F_s} \tag{11}$$

where F_{c2} is the wave force of a single pile in the pile group arranged in the vertical wave direction, and F_s is the wave force of a single pile.

The value of K_{cp} could not be found in the specifications or standards currently. In this paper, it can be assumed that K_{cp} between each row of piles in the parallel wave direction is the same according to Section 3. For each column of piles in a perpendicular wave direction, K_{cp} can be selected according to the front and rear positions of the piles. The cap-interference coefficient of the front row pile can be linearly interpolated according to the length d_b of the back side pile cap according to Figure 8. Similarly, the cap-interference coefficient of the back row pile can be linearly interpolated according to the length d_f of the front side pile cap according to Figure 9. Considering that the pile cap has a stronger interference effect on the peak wave force and a weaker interference effect on the valley value, the interference coefficient of the valley value can be taken safely. A more unfavorable value can be obtained for the pile groups with more than two columns.

5. Engineering Project Application of a Sea-Crossing Bridge

To verify the accuracy of the modified theoretical formula and the feasibility of the numerical water flume, we selected a sea-cross bridge as the project background in this section and compared the theoretical calculation formula with numerical results.

5.1. Project Description

5.1.1. Overview of Bridge and Foundation Structure

The engineering background selected in this section is the pile-group foundation structure of Xinghua Bay Bridge. The Xinghua Bay Bridge Section includes two main channels, Mulanxi and Diluxi. The schematic diagram of the bridge site is shown in Figure 15.

Figure 15. Geographical location of the bridge.

The main bridge is a four-span variable cross-section steel structure, and the approach bridge is a four-span continuous beam bridge. The pile-group foundation structure of the main bridge has two arrangement forms. The foundation of the three piers of the two main spans is an integrated pile-group structure with two rows and seven columns. The side span foundation includes two split pile groups arranged in two rows and two columns. The caps of the above foundations are square caps. The schematic diagram is shown in Figure 16a,b. The approach section close to the side span also adopts two split pile-group structures with two rows and two rows, and the rest adopt two single-row pile foundation structures, as shown in Figure 16c,d.

The dimensions of the above four pile-group foundations are shown in Table 9.

Table 9. The dimensions of the four pile-group foundations (m).

	D	$b \times l$	h	l_l	l_t	d_l	d_t	l_c
Main span	2.5	34.5 × 11.4	4.5	6	5	2.7	2.25	integration
Side span	2.2	10 × 8.8	3.5	5.2	6.2	1.8	1.9	8
Approach bridge close to the side span	1.8	9 × 6.9	2.5	3.6	5.5	1.65	1.75	9
Others	2.5	13 × 4	2.5	-	9	2	2	5

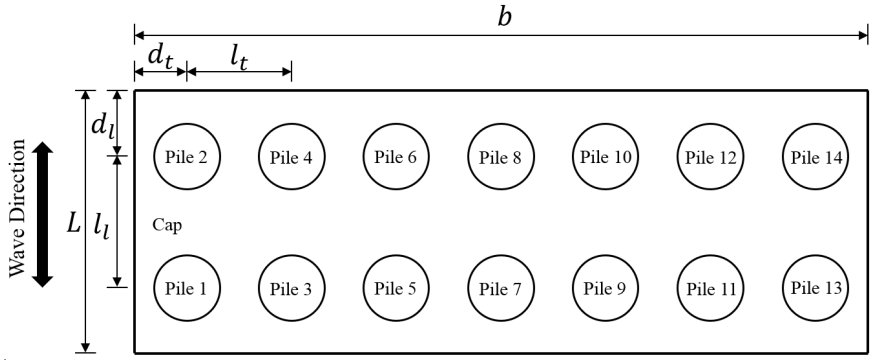

(**a**) Foundation of the main span

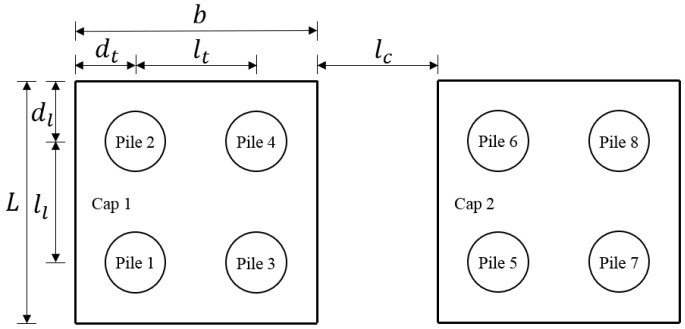

(**b**) Foundation of side span

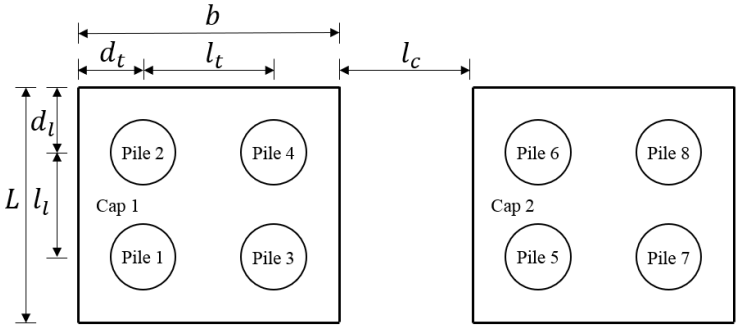

(**c**) Foundation of approach section close to side span

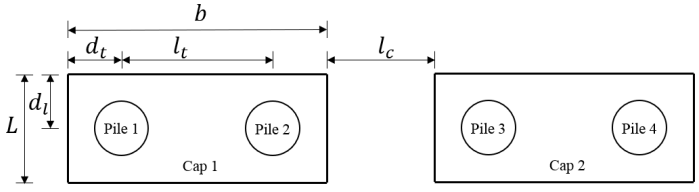

(**d**) Others

Figure 16. Schematic diagram of pile-group foundation.

5.1.2. Statistics of Wave Parameters at the Bridge Site

The wave characteristics in this area are mainly mixed waves dominated by the monsoon. The wave height distribution with a recurrence period of 100 years is shown in Figure 17.

The wave parameters of the above four pile-group foundations are shown in Table 10. To simplify the simulation, the water level is selected as the pile cap is half submerged, and the water depth is safely set as the water depth after 5 m of silt scouring at each foundation.

Table 10. The wave parameters of the above foundations.

Case	Significant Wave Height H/m	Significant Period T/s	Depth$d$/m	Water-Level Coefficient C_W
Main span	2.20	9.00	10.35	0.5
Side span	2.16	8.97	9.65	0.5
Approach bridge close to the side span	2.09	8.91	8.75	0.5
Others	2.09	8.91	8.75	0.5

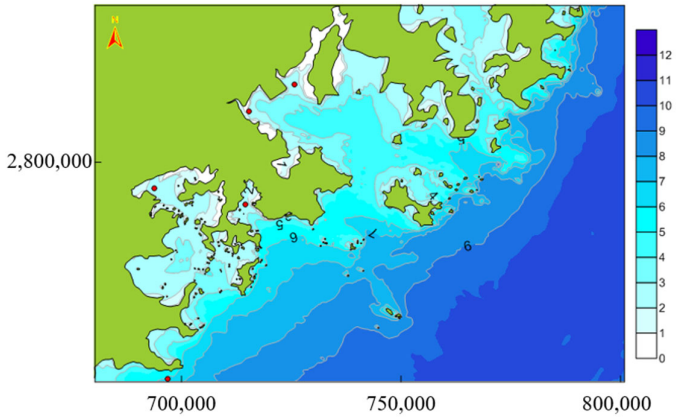

Figure 17. Wave height distribution (m).

5.2. Comparison of the Modified Theoretical Results, Numerical Simulation, and Specification Values

5.2.1. Parameter Selection of Theoretical Formula

We need to determine the value of K_{cp}, K_s, and K_I in Equation (9). As described in Section 4, K_{cp} can be interpolated from the fitting formula in Figures 11 and 12, considering the dimensions of the different foundations, shown in Table 11.

Table 11. The cap-interference coefficient K_{cp} under four cases.

Case	Front Row	Back Row
Main span	0.813	0.791
Side span	0.822	0.803
Approach bridge close to the side span	0.830	0.813
Others	0.900	

Similarly, the corresponding shelter and interference coefficients can be obtained through the linear fitting of the pile-group coefficients. For simplicity, only the results obtained are shown in Table 12.

Table 12. Shelter coefficient and interference coefficient of four foundations.

Case	Shelter Effect Coefficient K_S	Interference Effect Coefficient K_I	
		Pile on One Side	Piles on Both Sides
Main span	0.922	1.120	1.210
Side span	0.921	1.063	
Approach bridge close to the side span	0.910	1.047	
Others	1.000	1.020	

5.2.2. The Pile-Group Foundations Model and Three-Dimensional Numerical Wave Flume

The wave forces for the four groups of pile foundations were simulated using a three-dimensional numerical wave flume. The flume's length measures 250 m, its height is 15 m, and the main span has a width of 60 m, while the side span measures 50 m widthwise. In order to gauge the most unfavorable situation, the angle of attack for the waves was maintained perpendicular to the bridge's direction. Figure 18 displays the horizontal velocity contour of the wave surface at a specific time under the main span situation, and the meshing is shown in Figure 19.

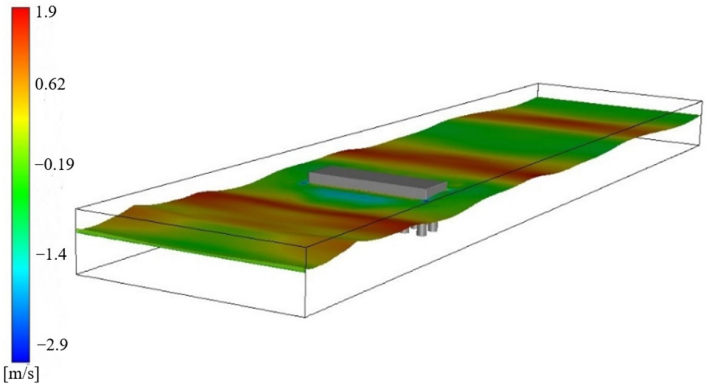

Figure 18. Numerical wave flume of the main span.

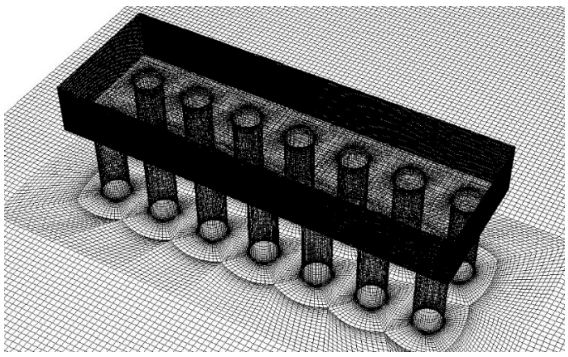

Figure 19. Meshing of the main span.

5.2.3. Results Analysis

For the above pile-group foundation structure, the relevant specification [38] can be used to calculate the wave force of the pile group. The shelter effect coefficient and influence effect coefficient given in the specification can be obtained by the interpolation method, as shown in Table 13. In addition, there is no provision for K_{cp} in the specification; the values in Table 11 are used.

Table 13. Shelter coefficient and interference coefficient of four foundations in the specification [38].

Case	Shelter Effect Coefficient K_S	Interference Effect Coefficient K_I
Main span	1.000	1.500
Side span	1.000	1.255
Approach bridge Close to the side span	1.000	1.194
Others	1.000	1.140

The results of the modified theoretical formula are compared with the specification value and the numerical simulation results, as shown in Figure 20. The foundations of the side span and the approach bridge are split caps. The comparison of the results in a diagram is only the wave-force time history under the same case.

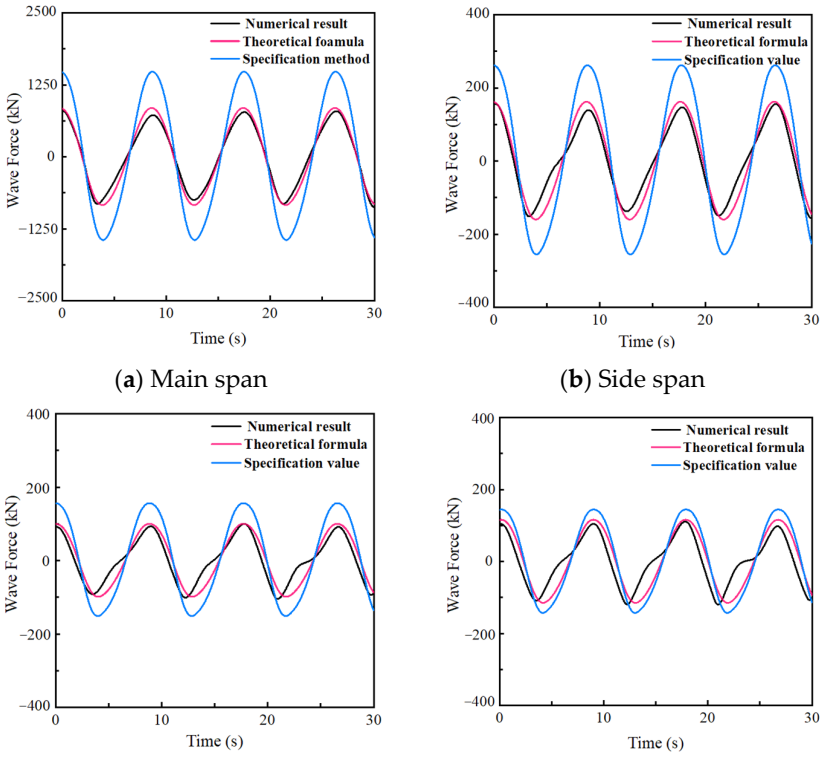

Figure 20. Comparison of wave-force time history.

The peak value of the wave-force time history of the pile-group structure is selected, and the average value is calculated. By comparing the results of the theoretical formula value and the numerical result, the safety amplification factor k_A can be obtained:

$$k_A = \frac{F_C}{F_N} \tag{12}$$

where F_C is the maximum wave force from the theoretical formula, and F_N is the maximum horizontal wave force from the numerical flume. The safety amplification coefficients of the above four cases are calculated as shown in Table 14.

Table 14. Safety amplification coefficients of four cases.

Case	Theoretical Formula Value/kN	Numerical Result/kN	Safety Amplification Coefficients
Main span	878	796	1.10
Side span	168	152	1.09
Approach bridge close to the side span	96	92	1.04
Others	116	101	1.15

Table 13 reveals that the wave forces calculated through the theoretical formula are in good agreement with the numerical simulation results. This highlights the fact that the theoretical formula has certain feasibility. At the same time, the wave forces calculated by Chinese specification will be significantly greater than the results of the numerical simulation and theoretical formula, indicating that these recommended values are relatively conservative.

6. Conclusions

In this paper, a three-dimensional numerical wave flume is established to investigate the influence of the cap on wave forces acting on pile groups. The setup of the flume, including wave generation and elimination, the grid size, and the boundary conditions, has been validated with the test results of the physical flume in the relevant literature. The influence of the cap on the pile groups with different arrangements and water levels was studied. The cap-interference coefficient K_{cp} was defined, and its variation law was given. It was found that for the single row of piles perpendicular to the wave, the center distance of the pile and the width of the cap have little effect on K_{cp}. Meanwhile, for the single row of piles parallel to the wave, the cap length before and after the pile has a negative correlation with K_{cp}. The law of multi-row piles is similar to that of single-row piles.

We proposed a modified theoretical formula with K_{cp} for calculating wave forces on piles as a theoretical formula for calculating wave forces considering the cap effects. Based on the parametric analysis mentioned earlier, the recommended value of K_{cp} was given.

After that, four groups of pile-foundation structures in engineering projects were selected to verify the feasibility of numerical flumes in practical engineering. Comparing the results of the pile-group wave force calculated by the numerical water flume, specification value, and theoretical formula, it is concluded that the results from the numerical water flume are in good agreement with that of the theoretical formula, while the results of the specification value are more conservative. The methods used in this article and the obtained variation laws can provide a reference for engineering.

However, due to limitations in computer power and time, we were unable to calculate many different cases with different sizes of caps, resulting in certain limitations in the formula. At the same time, caps are not only square, but may also have shapes such as circles and triangles, which can be further explored in the future.

Author Contributions: Conceptualization, R.M.; methodology, R.M. and H.C.; software, R.M., H.C. and Z.H.; validation, Y.L., H.C. and Z.H.; formal analysis, Y.L. and Z.H.; investigation, Y.L. and Z.H.; writing—original draft preparation, R.M., Y.L. and H.C.; writing—review and editing, R.M. and H.C.; supervision, R.M.; funding acquisition, H.C. All authors have read and agreed to the published version of the manuscript.

Funding: This work was supported by the National Natural Science Foundations of China [grant number 52238005], Shanghai Pujiang Program [grant number 22PJD079], China Postdoctoral Science Foundation [grant number 2022M722426].

Institutional Review Board Statement: Not applicable.

Informed Consent Statement: Not applicable.

Data Availability Statement: The data presented in this study are available on request from the corresponding author.

Conflicts of Interest: The authors declare that they have no known competing financial interests or personal relationships that could have appeared to influence the work reported in this paper.

References

1. Liu, H. Hydrodynamic Problems Associated with Construction of Sea-Crossing Bridges. *J. Hydrodyn.* **2006**, *18*, 13–18. [CrossRef]
2. Fang, C.; Tang, H.J.; Li, Y.L.; Wang, Z.W. Effects of random winds and waves on a long-span cross-sea bridge using Bayesian regularized back propagation neural network. *Adv. Struct. Eng.* **2020**, *23*, 733–748. [CrossRef]
3. Okeil, A.M.; Cai, C.S. Survey of short- and medium-span bridge damage induced by Hurricane Katrina. *J. Bridge Eng.* **2008**, *13*, 377–387. [CrossRef]
4. Haney, J.P.; Herbich, J.B. Wave Flow around Thin Piles and Pile Groups. *J. Hydraul. Res.* **1982**, *20*, 1–14. [CrossRef]
5. Fredsoe, J. Turbulent Boundary-Layer in Wave-Current Motion. *J. Hydraul. Eng.-Asce* **1984**, *110*, 1103–1120. [CrossRef]
6. Kemp, P.H.; Simons, R.R. The Interaction Between Waves and a Turbulent Current—Waves Propagating with the Current. *J. Fluid Mech.* **1982**, *116*, 227–250. [CrossRef]
7. O'Brien, M.P.; Morison, J.R. The forces exerted by waves on objects. *Eos Trans. Am. Geophys. Union* **1952**, *33*, 32–38. [CrossRef]
8. Sarpkaya, T. *Wave Forces on Offshore Structures*; Cambridge University Press: Cambridge, UK, 2010.
9. Justesen, P. Hydrodynamic-Forces on Large Cylinders in Oscillatory Flow. *J. Waterw. Port Coast. Ocean. Eng.-Asce* **1989**, *115*, 497–514. [CrossRef]
10. Sarpkaya, T. Forces on Cylinders near a Plane Boundary in a Sinusoidally Oscillating Fluid. *J. Fluids Eng.-Trans. Asme* **1976**, *98*, 499–505. [CrossRef]
11. Boccotti, P.; Arena, F.; Fiamma, V.; Barbaro, G. Field experiment on random wave forces acting on vertical cylinders. *Probabilistic Eng. Mech.* **2012**, *28*, 39–51. [CrossRef]
12. MacCamy, R.C.; Fuchs, R.A. *Wave Forces on Piles: A Diffraction Theory*; US Beach Erosion Board: San Francisco, CA, USA, 1954.
13. Neelamani, S.; Sundar, V.; Vendhan, C.P. Dynamic Pressure Distribution on a Cylinder Due to Wave Diffraction. *Ocean Eng.* **1989**, *16*, 343–353. [CrossRef]
14. Garrison, C.J.; Chow, P.Y. Wave Forces on Submerged Bodies. *J. Waterw. Harb. Coast. Eng. Div.* **1972**, *98*, 375–392. [CrossRef]
15. Terro, M.J.; Abdel-Rohman, M. Wave induced forces in offshore structures using linear and nonlinear forms of Morison's equation. *J. Vib. Control* **2007**, *13*, 139–157. [CrossRef]
16. Liu, S.X.; Li, Y.C.; Li, G.W. Wave Current Forces on the Pile Group of Base Foundation for the East Sea Bridge, China. *J. Hydrodyn.* **2007**, *19*, 661–670. [CrossRef]
17. Qu, J.Z.; Xue, L.P.; Wang, B.L.; Ni, X. Unified empirical relations for total inline wave forces on pile-supported structures in regular and irregular waves. *Ocean Eng.* **2017**, *145*, 200–206. [CrossRef]
18. Zhang, H.C.; Liu, S.X.; Li, J.X.; Fan, Y.P. Experimental study on short-crested random wave interaction with pile group in double-row side-by-side arrangement: A statistical analysis. *Coast. Eng. J.* **2020**, *62*, 236–251. [CrossRef]
19. Zhang, H.C.; Liu, S.X.; Li, J.X.; Zhang, R.L.; Hao, J. Interactions between multi-directional irregular waves and a pile group in a side-by-side arrangement: Statistical analysis. *Coast. Eng.* **2019**, *147*, 115–134. [CrossRef]
20. Bonakdar, L.; Oumeraci, H.; Etemad-Shahidi, A. Wave load formulae for prediction of wave-induced forces on a slender pile within pile groups. *Coast. Eng.* **2015**, *102*, 49–68. [CrossRef]
21. Liu, P.L.F.; Losada, I.J. Wave propagation modeling in coastal engineering. *J. Hydraul. Res.* **2002**, *40*, 229–240. [CrossRef]
22. Dong, C.M.; Huang, C.J. Generation and propagation of water waves in a two-dimensional numerical viscous wave flume. *J. Waterw. Port Coast. Ocean. Eng.* **2004**, *130*, 143–153. [CrossRef]
23. Huang, B.; Zhu, B.; Cui, S.G.; Duan, L.L.; Cai, Z.L. Influence of Current Velocity on Wave-Current Forces on Coastal Bridge Decks with Box Girders. *J. Bridge Eng.* **2018**, *23*, 04018092. [CrossRef]
24. Deng, L.W.; Yang, W.L.; Li, Q.; Li, A. CFD investigation of the cap effects on wave loads on piles for the pile-cap foundation. *Ocean Eng.* **2019**, *183*, 249–261. [CrossRef]
25. Patankar, S. *Numerical Heat Transfer and Fluid Flow*; CRC Press: Boca Raton, FL, USA, 2018.
26. Prasad, D.D.; Ahmed, M.R.; Lee, Y.H.; Sharma, R.N. Validation of a piston type wave-maker using Numerical Wave Tank. *Ocean Eng.* **2017**, *131*, 57–67. [CrossRef]
27. Finnegan, W.; Goggins, J. Numerical simulation of linear water waves and wave-structure interaction. *Ocean Eng.* **2012**, *43*, 23–31. [CrossRef]
28. Orszag, S.A.; Yakhot, V. Renormalization group analysis of turbulence. In Proceedings of the International Congress of Mathematicians, Berkeley, CA, USA, 3–11 August 1986.
29. Koushan, K.; Krasilnikov, V.; Nataletti, M.; Sileo, L.; Spence, S. Experimental and Numerical Study of Pre-Swirl Stators PSS. *J. Mar. Sci. Eng.* **2020**, *8*, 47. [CrossRef]
30. Hirt, C.W.; Nichols, B.D. Volume of Fluid (Vof) Method for the Dynamics of Free Boundaries. *J. Comput. Phys.* **1981**, *39*, 201–225. [CrossRef]
31. Schlichting, H.; Gersten, K. *Boundary-Layer Theory*; World Book Publishing Company: Chicago, IL, USA, 2017.

32. Mo, W.H.; Irschik, K.; Oumeraci, H.; Liu, P.L.F. A 3D numerical model for computing non-breaking wave forces on slender piles. *J. Eng. Math.* **2007**, *58*, 19–30. [CrossRef]
33. Xiang, T.; Istrati, D. Assessment of Extreme Wave Impact on Coastal Decks with Different Geometries via the Arbitrary Lagrangian-Eulerian Method. *J. Mar. Sci. Eng.* **2021**, *9*, 1342. [CrossRef]
34. Celebi, M.S.; Kim, M.H.; Beck, R.F. Fully nonlinear 3-D numerical wave tank simulation. *J. Ship Res.* **1998**, *42*, 33–45.
35. Romate, J.E. Absorbing Boundary-Conditions for Free-Surface Waves. *J. Comput. Phys.* **1992**, *99*, 135–145. [CrossRef]
36. Fenton, J.D. The Numerical-Solution of Steady Water-Wave Problems. *Comput. Geosci.* **1988**, *14*, 357–368. [CrossRef]
37. Wang, Z.G.; Qiu, W.L. Characteristics of wave forces on pile group foundations for sea-crossing bridges. *Ocean Eng.* **2021**, *235*, 109299. [CrossRef]
38. Xie, S.L.; Shao, S.L.; Zhang, S.H. *Code of Hydrology for Sea Harbour*; Communications Press Corporation Limited: Beijing, China, 2013.